Optimization of the Design and Operation of FAIMS Analyzers

Alexandre A. Shvartsburg, Keqi Tang, and Richard D. Smith
Biological Sciences Division, Environmental Molecular Sciences Laboratory, Pacific Northwest National Laboratory, Richland, Washington, USA

Field asymmetric waveform ion mobility spectrometry (FAIMS) holds significant promise for post-ionization separations in conjunction with mass-spectrometric analyses. However, a limited understanding of fundamentals of FAIMS analyzers has made their design and operation largely an empirical exercise. Recently, we developed an a priori simulation of FAIMS that accounts for both ion diffusion (including anisotropic components) and Coulomb repulsion, and validated it by extensive comparisons with FAIMS/MS data. Here it is corroborated further by FAIMS-only measurements, and applied to explore how key instrumental parameters (analytical gap width and length, waveform frequency and profile, the identity and flow speed of buffer gas) affect FAIMS response. We find that the trade-off between resolution and sensitivity can be managed by varying gap width, RF frequency, and (in certain cases) buffer gas, with equivalent outcome. In particular, the resolving power can be approximately doubled compared to "typical" conditions. Throughput may be increased by either accelerating the gas flow (preferable) or shortening the device, but below certain minimum residence times performance deteriorates. Bisinusoidal and clipped-sinusoidal waveforms have comparable merit, but switching to rectangular waveforms would improve resolution and/or sensitivity. For any waveform profile, the ratio of two between voltages in high and low portions of the cycle produces the best performance. (J Am Soc Mass Spectrom 2005, 16, 2–12) © 2004 American Society for Mass Spectrometry

Separation of gas-phase ionic mixtures by field asymmetric waveform ion mobility spectrometry (FAIMS) extends back over a decade in the technical literature [1–3], but has attracted a broad interest in the analytical and mass-spectrometry communities only recently [4–29]. FAIMS separates ions by the difference between mobilities at high (K_H) and low (K_L) electric fields, in other words the average slope of mobility as a function of field, $K(E)$. The form of $K(E)$ may be complex: with increasing E, mobilities (of both cations and anions) may increase (termed species of Type A), decrease (Type C), or initially increase, but decrease at yet higher E (Type B) [4, 5]. Usually, small and structurally rigid species belong to Type A and large flexible ones (e.g., proteins) belong to Type C. $K(E)$ can be represented by a polynomial of even powers of E/N:

$$K(E) = K(0)(1 + a(E/N)^2 + b(E/N)^4 + c(E/N)^6 + \ldots), \quad (1)$$

At moderately high E/N relevant to FAIMS (up to ~60–80 Td), eq 1 can usually be truncated after the $b(E/N)^4$ term [6–8].

Experimentally, a gas stream entraining ions passes between two electrodes that carry a time-dependent potential $V_D(t)$ that alternates between "high" and "low" voltages, such that the integral value over the cycle is null but time-averaged positive and negative voltages differ [4, 5]. Then only a hypothetical ion with constant $K(E)$ would be transmitted, while species exhibiting variable $K(E)$ drift towards one of the electrodes and eventually neutralize upon impact [4, 5]. For a particular ion, this may be prevented by applying a specific DC compensation voltage (CV) on top of $V_D(t)$ so as to exactly offset the systematic drift generated by $V_D(t)$. A CV spectrum for ionic mixture could be acquired by scanning the CV across a reasonable range of values, similarly to scanning a quadrupole filter when obtaining a mass spectrum [4, 5].

Two key developments of the late 1990s that fashioned FAIMS into a major analytical tool were (1) the advent of concentric cylinder design [3] and (2) coupling to MS [4, 5]. Cylindrical devices are often more sensitive than earlier parallel planar designs [1] due to an ion focusing effect (discussed below). Coupling FAIMS to MS has opened a range of new analytical and bioanalytical applications. As with the other gas-phase separations technique of ion mobility spectrometry (IMS) [30–33], a major attraction of FAIMS is high speed that allows high-throughput analyses. In particular, it enables fast two-dimensional separations, such as LC/FAIMS/MS on the timescale of single-stage LC separations.

Published online November 23, 2004

Address reprint requests to Dr. R. D. Smith, Biological Systems Analysis and Mass Sepctrometry, Pacific Northwest National Laboratory, 3335 Q Avenue (K8-98), P.O. Box 999, Richland, WA 99352, USA.

1044-0305/05/$30.00
doi:10.1016/j.jasms.2004.09.009

Received July 21, 2004
Revised September 9, 2004
Accepted September 10, 2004

While FAIMS technology has already shown a potential for diverse applications (e.g., in environmental monitoring [6, 9–13], security [14], drug screening [15–17], product quality control [18], natural resource management [19], and medical research [20]), its utility would certainly be increased and broadened by improved resolution, sensitivity, and throughput. The priority of each depends on the application. The resolving power of FAIMS has been limited to ~10–30 (versus >100 for drift tube IMS [33]). This is often insufficient: for example, FAIMS of typical proteolytic digests generally separates different charge states of peptides, but not peptides of the same charge state (which would benefit proteomics analyses) [21]. Likewise, distinguishing between HSO_4^- and ClO_4^- or between phthalic acid anion isomers is a challenge [6, 22]. For FAIMS/MS, sensitivity is determined by the efficiency of ion transmission to the MS. In cylindrical FAIMS, this efficiency is enhanced through ion focusing by the inhomogeneous electric field created in the annular space between cylinders (analytical gap) [4, 5]. Still, signal losses are significant, especially for ions that do not focus well because of weak $K(E)$ dependence, i.e., ions having low absolute CV, $|CV|$ [11]. Reducing this discrimination is a challenge for quantitative analyses. The throughput of cylindrical FAIMS (~1 fraction/s) is high compared to condensed-phase techniques such as LC or CE, but low compared to IMS that may complete a separation in 1–100 ms. Considering the peak elution time from typical HPLC [34, 35], accelerating FAIMS analyses would be valuable for LC/FAIMS coupling.

Whichever parameter one desires to optimize, a comprehensive realistic model for ion dynamics in FAIMS analyzers (equivalent to "SIMION" [36] in MS) would be of great value. Efforts to construct such a model were initiated by Guevremont and coworkers [5, 23, 24] who propagated ion trajectories under the influence of $V_D(t)$. Those simulations helped the understanding of ion focusing and trapping in cylindrical and hemispherical [23, 24] FAIMS geometries. However, that model incorporated neither ion diffusion nor space-charge effects, rendering it unable to describe the resolution or sensitivity of analyses.

Recently, we developed a classical molecular dynamics simulation accounting for both effects [37]. This treatment has successfully reproduced the resolution and sensitivity of FAIMS/MS analyses for numerous systems [37]. The model has subsequently been expanded to handle separations in gas mixtures [38]. High-field ion mobilities in mixtures of disparate gases significantly deviate from Blanc's law, which often augments the difference between K_H and K_L and thus improves the resolution and peak capacity [38]. Here, we further validate this model by comparison with pure FAIMS measurements and then apply it to elucidate the dependence of FAIMS response on pertinent mechanical and operational parameters.

Computational Treatment

The numerical procedure of present simulations has been described [37]. Briefly, an ensemble of ion trajectories is propagated through cylindrical FAIMS by integrating elementary displacements along the radial coordinate r due to three phenomena: external electric field created by $\{V_D(t) + CV\}$, diffusion of ions in the buffer gas, and their mutual Coulomb repulsion. The form of $V_D(t)$ is arbitrary. Here we consider all three waveforms used in FAIMS to date: the sum of sinusoidal and its scaled phase-shifted harmonic [8] (Figure 1a) that is most common

$$V_D(t) = [f \sin wt + \sin(hwt - \varphi)]V_{max}/(f + 1), \quad (2)$$

a rectangular waveform tried in a FAIMS-R1 prototype [5] (Figure 1b):

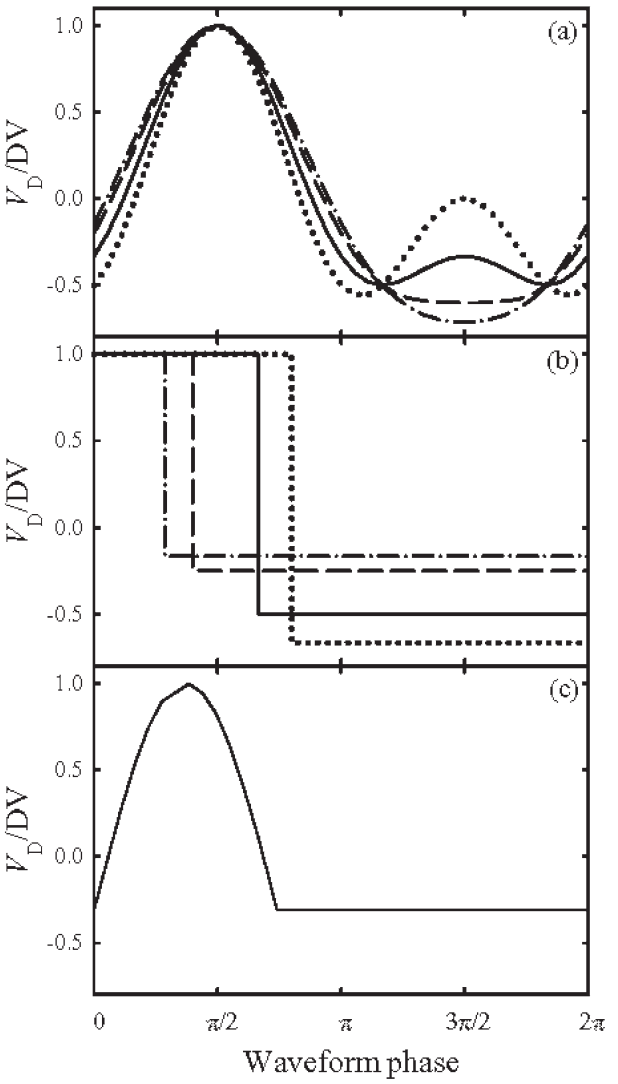

Figure 1. Asymmetric waveforms considered in this study: bisinusoidal from superpositions of a sinusoidal and scaled 2nd harmonic (**a**), rectangular (**b**), and clipped sinusoidal (**c**). In (**a**) and (**b**), the high-to-low coefficients f are: solid line–2, dash–4, dash dot–6, dotted–1.0 in (**a**) and 1.5 in (**b**). In (**c**), f = 1.7.

$$V_D(t) = V_{max} \text{ for } \{0 < t \le t_c/(f+1)\};$$
$$V_D(t) = -V_{max}/f \text{ for } \{t_c/(f+1) < t \le t_c\}, \quad (3)$$

and a recently introduced clipped displaced sinusoidal [39–42] (Figure 1c):

$$V_D(t) = \left[\pi t_c \sin(\pi t/t_s) - 2t_s\right] V_{max}/(\pi t_c - 2t_s)$$

for $\{0 < t \le t_s\}$;

$$V_D(t) = -2t_s V_{max}/(\pi t_c - 2t_s) \text{ for } \{t_s \le t \le t_c\}; \quad (4)$$

In eqs 2–4, V_{max} is the highest instantaneous voltage—the "dispersion voltage" (DV). In eq 2, we use $h = 2$ and $\varphi = \pi/2$ adopted in all FAIMS work [8]. For the "high-to-low ratio" f, values of 2, 3, and 4 have been used, with most data published for $f = 2$. We optimize FAIMS performance as a function of f in the section, "Optimization of Asymmetric Waveform Profile," elsewhere $f = 2$ is assumed. In eqs 3, 4, t_c is the duration of waveform cycle, $t_c = 2\pi/w$. In eq 4, t_s is the duration of unclipped sinusoidal waveform, then f may be defined as $(t_c - t_s)/t_s$. The model for diffusion accounts for high-field (non-thermal) and anisotropic contributions that increase the effect under typical FAIMS conditions significantly [37]. Ions impacting the electrodes (internal at $r = R_{in}$ or external at $R = R_{out}$) are removed, and the ion count continually drops as the simulation progresses. Calculations can begin from any distribution of ions across the analytical gap [37]. In this work, we adopted the initial conditions with all ions at the gap median. Initial ensembles involved n = 300–30,000 ions, with higher n necessary for sufficient statistics of ions passing FAIMS in cases of poor transmission. Since modeling of the space-charge effect requires accounting for all pairwise interactions [37], part of computation scales as n^2 and simulations for high n are expensive.

The output of calculation is the ion current exiting the device (I_{out}) as a fraction of input current (I_{in}). This fraction plotted versus CV (at a particular DV) determines the peak profile that has a certain full width at half maximum [37] (FWHM). By definition, the ratio of peak CV to FWHM is the resolving power (R). The same fraction evaluated at a peak apex is the ion transmission efficiency [37], which allows one to calculate absolute I_{out} from a known I_{in}. The I_{out} current scales with I_{in} at very low I_{in}. As I_{in} increases, I_{out}/I_{in} ratio always decreases and eventually I_{out} reaches the saturation current, I_{sat} [37]. At that point, FAIMS becomes a current limiter: further raise of I_{in} does not affect I_{out} as excess ions are eliminated in a "Coulomb explosion" early in the simulation. The level of I_{sat} in cylindrical FAIMS strongly depends on the slope of $K(E)$ that determines the strength of ion focusing. Typical values for polyatomic ions are ~10–100 pA, i.e., below I_{in} normally produced by ESI unless from dilute samples [43]. Thus FAIMS often operates in a saturated regime, where I_{out} is calculable without regard to I_{in}. The form of I_{out}(DV) may be related to that of the signal observed in FAIMS/MS [37], while absolute I_{out} may be compared with direct measurements of ion current appearing from FAIMS.

Validation of Simulations for Stand-Alone FAIMS

The present model has been corroborated by resolution and sensitivity data for analytes ranging from small inorganic ions to whole proteins, including cations and anions, and species of both A- and C-types [37]. Altogether, these ions pass FAIMS in three out of four possible modes: P1, P2, and N1. While those comparisons have demonstrated the accuracy and robustness of our computational approach for diverse systems and conditions, they refer to experimental data from FAIMS coupled to MS, either quadrupole or TOF. An MS stage may distort FAIMS separation characteristics, in particular by limiting the ion current downstream of FAIMS because of finite charge capacity of MS elements such as quadrupoles [44] and/or detector saturation [37]. This would flatten the true dependence of ion transmission through FAIMS on DV, and broaden apparent features in CV spectra by disproportionately clipping the ion intensity at peak apexes.

Hence simulations should also be compared with direct results of FAIMS separations not affected by subsequent ion handling. These data are available from the stand-alone FAIMS device, known as FAIMS-E [4, 5, 27] or the field ion spectrometer [3], where the (not mass-selected) ions are recorded using an electrometer installed immediately past the device. This mode is of utility in the field and other settings where the equipment portability, footprint, power requirements, or cost are primary concerns. To evaluate the simulation in that scenario, we model FAIMS-E data for $H^+(H_2O)_n$ protonated water clusters [5]. Unless indicated otherwise, simulations below are in N_2 (under saturated conditions) for typical instrumental parameters [37] (R_{in} = 7 mm, R_{out} = 9 mm, gap length = 90 mm, DV = ±3.3 kV, $w_c = w/2\pi$ = 210 kHz, and ion residence time equal to 0.2 s) [37]. The mobility characteristics assumed for all ions are in Table 1. To compare data for different g, CV and/or DV axes in some figures are converted respectively to "compensation field", E_C = (CV)/g and "dispersion field", E_D = (DV)/g.

The CV peak profiles calculated across the experimental range of DV are in an excellent agreement with measurements (Figure 2). This verifies (Figure 2a) that the model produces good CV spectra not only at the highest DV (>3 kV) that are generally optimal [37], but also at lower DV (many applications involve measurements across a range of DV). Further, the relative sensitivity computed as a function of DV closely reproduces the measurements [5] (Figure 2c). The agreement in Figure 2 is better than that found previously [37], and same is true when the clipped sinusoidal waveform (eq

Table 1. Mobility parameters assumed for the ions modeled in this work[a]

System	$K_0(0)$, $cm^2/(Vs)$	a, Td^{-2}	b, Td^{-4}
$H^+(H_2O)_n$ in air[b]	2.10	2.02×10^{-5}	-3.38×10^{-10}
(Leucine − H)$^-$ in air[c]	2.00	5.43×10^{-6}	-1.85×10^{-10}
$(H^+)_{12}$bovine ubiquitin[d] (major conformer) in N_2	1.20	-2.34×10^{-6}	-1.6×10^{-12}
Cs^+ in N_2[e]	2.21	9.88×10^{-6}	-2.76×10^{-10}
Cs^+ in CO_2[f]	0.95	1.31×10^{-5}	-3.52×10^{-10}
I^- in air[g]	2.10	1.19×10^{-5}	-7.4×10^{-10}

[a]Values of $K_0(0)$ listed here for (Leucine − H)$^-$ and $(H^+)_{12}$bovine ubiquitin are ~ 10% lower than entries in Table 1 of reference [37]. This does not mean any difference of $K(0)$ actually employed in calculations, but reflects a nomenclature error in [37], where $K(0)$ used in simulations under experimental conditions (T = 25 °C) were termed $K_0(0)$ that are defined as mobilities reduced to 0 °C. All mobilities given here are properly reduced to 0 °C, e.g., $K_0(0)$ = 2.0 for (Leucine − H)$^-$ means $K(0)$ = 2.18 used in the model. With regard to other $K_0(0)$ in [37], those for H^+tryptophan, H^+glycine, and HSO_4^- should have been given as 1.91, 2.12, and 2.29 $cm^2/(Vs)$, respectively. Those values are in a good agreement with available IMS data, significantly better than that for inaccurate $K_0(0)$ listed in [37]. For example, $K_0(0)$ ~2.3 $cm^2/(Vs)$ for HSO_4^- in air is quite reasonable in view of the measurements for similar anions like $H_2NO_4^-$, $H_2CO_4^-$, and CO_4^- in N_2 and O_2 [46,47].
[b]$K_0(0)$ is from reference [48] and *a*, *b* were derived from measured CVs [5]. To evaluate the longitudinal diffusion coefficient [37], we assumed n = 3 (m = 55 u). Typically, n = 2 or 3 [48]; the result is not significantly dependent on the choice.
[c]Data from reference [8]
[d]$K_0(0)$ is from references [28, 29, 49]; *a*, *b* were derived from measured CVs [29].
[e]$K_0(0)$ is from references [50]; *a*, *b* were derived from measured CVs [7].
[f]$K_0(0)$ is from reference [51] (measurements at ambient conditions); *a*, *b* were derived from measured CVs [7].
[g]$K_0(0)$ is extrapolated from the measurements for Cl^- (~ 2.9) [52] and Br^- (~ 2.5) [53]; *a*, *b* are from reference [39].

4) is used. This may simply reflect a much higher ion count in FAIMS-E providing better statistics, or indicate signal distortions in the MS analyzer, in which case any FAIMS simulation should be better for FAIMS-E than for FAIMS/MS.

Calculations and FAIMS-E experiments may be matched not just for relative ion intensities (Figure 2c), but also for absolute currents. From the few data available, measured values are aprroximately an order of magnitude below calculated I_{sat}: 10 pA versus $I_{sat} \approx$ 80 pA for H^+glycine [27] (at DV = 3 kV) and 9 pA versus $I_{sat} \approx$ 240 pA for $H^+(H_2O)_n$ (at DV = 2.6 kV) [5]. This appears reasonable, considering the competition for space-charge capacity from other co-injected species, inefficient extraction of ions from tubular FAIMS (with no hemispherical end), and a possibly incomplete ion collection by the external electrometer.

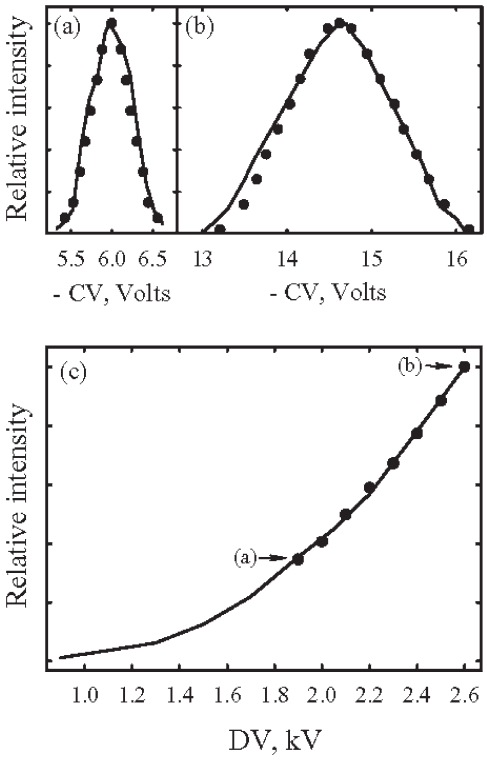

Figure 2. FAIMS-E response for $H^+(H_2O)_n$ ions: peak profiles at DV of 1.9 kV (**a**) and 2.6 kV (**b**), and relative sensitivity as a function of DV (**c**). Circles stand for measurements [5], lines are for calculations.

Optimization of Mechanical and Operational Parameters

Having the simulation of FAIMS analyzers extensively validated by diverse experimental data, we now apply it to optimize the design and functional parameters of these devices.

Analytical Gap Width and Waveform Frequency

The width of analytical gap (g) and waveform frequency (w_c) are key parameters governing the resolution and sensitivity of FAIMS analyses. The amplitude of periodic motion of ions during a FAIMS cycle is nearly proportional to $1/w_c$. As w_c drops, the turning points of oscillation move closer to electrodes, increasing ion losses and reducing transmission. When the oscillation amplitude exceeds g, all ions are neutralized in the first cycle. In effect, lowering w_c narrows the gap. This should improve the resolution as ions with trajectories displaced from the gap median (that form the shoulders of peaks in CV spectra) are destroyed disproportionately. A similar outcome (improving resolution while sacrificing sensitivity) may be achieved by reducing g. Three major questions arising from this are: (1) what is the maximum resolving power attainable in this process, (2) does it matter whether resolution is improved by decreasing g or w_c, and (3) how does the

nature of the analyte ion modify the effect of varying g and w_c?

To address these questions, we modeled the response of FAIMS with bisinusoidal waveform of eq 2 while varying g and w_c and fixing all other parameters. The gap width was adjusted while keeping the median radius equal to $(R_{in} + R_{out})/2$ so as to conserve the cylindrical curvature. To compare with previous calculations [37] at fixed g and w_c, simulations were performed for (Leucine − H)$^-$. In Figure 3a, saturated current is plotted as a function of g and w_c, in particular g = 2 mm used in most FAIMS devices to date, including the Ionalytics Selectra. As expected, I_{sat} increases for higher frequencies and wider gaps. There is a low-w_c cutoff that rises with narrowing of the gap, e.g., from $w_c \sim 40$ kHz at g = 3 mm to $w_c \sim 170$ kHz at g = 1.5 mm. However, below $g \sim 1.3$ mm no ions pass at any w: the diffusion and Coulomb repulsion push ions outside the band between R_{in} and R_{out} even when the magnitude of oscillations in FAIMS cycle approaches zero.

A decrease of w_c (at fixed g) improves the resolving power. For g = 2 mm, R triples from 8 at w_c = 750 kHz (used in Selectra) to 24 at w_c = 95 kHz (Figure 3b). For g = 1.5 mm, the resolution is higher to begin with and so improves less, from R = 17 at w_c = 750 kHz to R = 27 at w_c = 180 kHz (Figure 3c). Similar behavior was found for g = 3 mm. However, for a *fixed* I_{sat} the resolution is *independent* of g and w_c. As shown in Figure 3d, three disparate $\{g; w_c\}$ combinations yield similar $I_{sat} \sim 2$ pA and $R \sim 28$. This regime provides the best resolution but relatively low sensitivity, though an ion current of a few pA still suffices for many analytical needs. Other $\{g; w_c\}$ sets produce higher I_{sat} values, however two combinations yielding same I_{sat} also yield same (lower) R. Hence variations of gap width and waveform frequency are functionally equivalent, i.e., any desired trade-off of resolution versus sensitivity may be achieved by changing either parameter. In practice, varying w should be more convenient as it may be done via rapid electronic control rather than mechanical modifications.

While many FAIMS experiments involve saturated current conditions, in real analytical applications currents would normally be weaker. The response for (Leucine − H)$^-$ ions as a function of g and w_c in the zero-current limit ($I_{in} \rightarrow 0$) is modeled in Figure 4. The results closely resemble those in Figure 3, in particular we reach the parallel conclusion that the resolution at a *fixed* transmission efficiency is *independent* of the specific $\{g; w_c\}$ combination (as seen by matching the graphs in Figure 4b and c). Since the limiting cases in Figure 3 and Figure 4 bracket the full range of possibilities, the picture at any ion current should be similar.

How would varying g and w_c affect results for ions with different properties? For example, mobilities for large proteins are lower than those for small ions, e.g., $K(0)$ for major isomer of $(H^+)_{12}$ bovine ubiquitin (BU12) is ~60% of $K(0)$ for (Leucine − H)$^-$ (Table 1). More

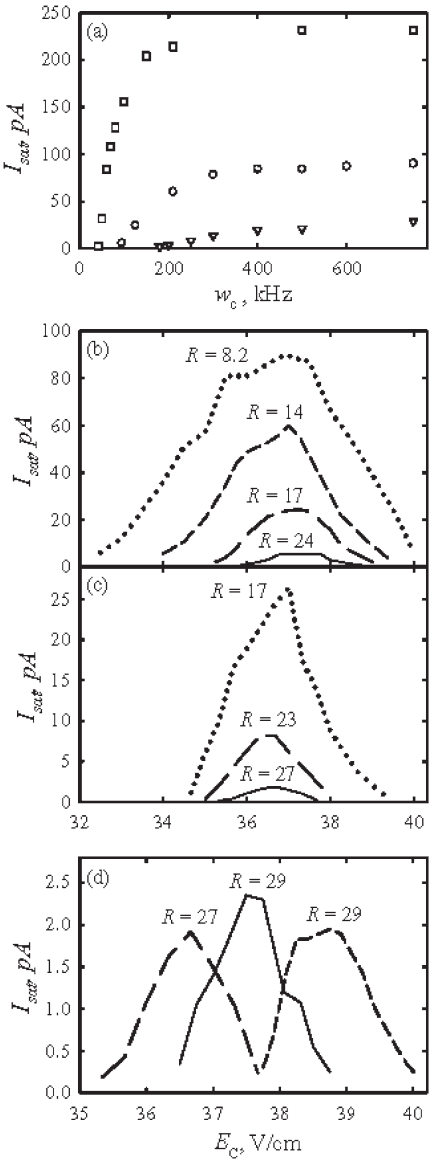

Figure 3. Simulated sensitivity (**a**) and resolution (**b**)–(**d**) of cylindrical FAIMS with a bisinusoidal waveform (f = 2, DV = −3.3 kV) as a function of gap width g and frequency w_c. All examples are for (Leucine − H)$^-$, under saturated conditions. Calculated resolving powers are given for all features. Transmitted currents in (**a**) are for g = 2 mm (circles), g = 3 mm (squares), and g = 1.5 mm (triangles). CV spectral profiles in (**b**) are for g = 2 mm, in (**c**) are for g = 1.5 mm. In (**b**), lines are for w_c = 750 kHz (dotted), 210 kHz (short dash), 125 kHz (long dash), and 95 kHz (solid). In (**c**), lines are for 750 kHz (dotted), 250 kHz (long dash), and 180 kHz (solid). Profiles in (**d**) are for g = 1.5 mm, w_c = 180 kHz (long dash), 2 mm, 86 kHz (solid), and 3 mm, 42 kHz (short dash).

importantly, the Einstein relationship between mobility and diffusion coefficient D at $E \rightarrow 0$ is:

$$D = k_B T K(E)/q, \quad (5)$$

where k_B is the Boltzmann constant, T is the temperature, and q is the ionic charge. Because of (+12) charge,

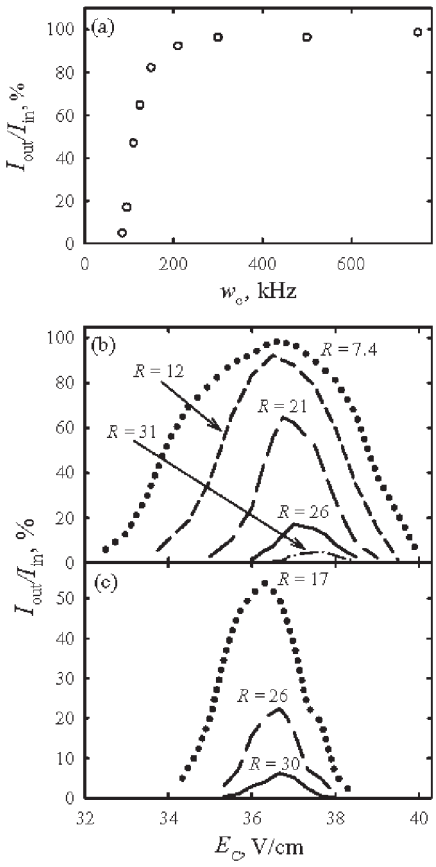

Figure 4. Same as Figure 3(**a**)–(**c**), but for the low-current limit ($I_{in} \rightarrow 0$). Panel (**a**) shows transmission efficiencies. In (**b**), the dash dot line is for w_c = 85 kHz. Other nomenclature is as in Figure 3.

D for BU12 is only 5% of that for (Leucine − H)$^-$. At high *E*, eq 5 is modified [37] and the value of *D* increases somewhat, still the diffusion of large multiply-charged protein ions generated by ESI is many times slower than their mobility suggests.

The result is a low diffusional loss of large multicharged proteins in FAIMS, despite their often weak *K*(*E*) dependence (Table 1) and thus modest focusing. This allows high ion currents and makes FAIMS passable with gaps narrower than those necessary for smaller ions (Figure 5). For example, the maximum current through a 2-mm gap (at w_c = 750 kHz) is >370 pA for BU12 versus only ~90 pA for (Leucine − H)$^-$, and a fair amount of BU12 passes even at g = 0.5 mm while the minimum g for (Leucine − H)$^-$ is ~1.3 mm as stated above. In part, this is due to BU12 having a lower mobility and thus a smaller oscillation amplitude than (Leucine − H)$^-$, but a very large difference in diffusion rates is still critical. This is demonstrated in Figure 5, showing I_{sat} for a hypothetical singly-charged ion with mass and *K*(*E*) of BU12. Maximum currents for that ion are lower than those for BU12 at any g and w_c, while the minimum g is greater. Thus a FAIMS device with a gap reduced to 0.5–1 mm could improve the resolution for intact protein analyses.

FAIMS Gas Medium

Most FAIMS work to date has used N_2 or air as the buffer gas. Gas mixtures (such as N_2/CO_2 and He/N_2) have shown promise as a FAIMS medium, often improving the instrumental resolution and sensitivity compared to either individual component [9, 15, 16, 18, 22, 29, 38]. This appears largely due to deviations from Blanc's law that may expand the peak capacity of separations [38]. The performance parameters of FAIMS analyses in gas mixtures will be discussed in a future publication, here we focus on the effect of interchanging pure gases.

Experimental data of that kind are meager: the only detailed report involves Cs^+ in several gases [7] (including N_2 and CO_2). The CV spectral peaks measured in CO_2 at any DV were unusually broad (FWHM about twice those of peaks in N_2), which is reproduced by present modeling: FWHM = 2.0× that in N_2. (According to experimental settings [7], these calculations were performed for R_{in} = 5 mm, R_{out} = 7 mm). The reason is that the mobility of Cs^+ in CO_2 is ~ 40% that in N_2 (Table 1), so the oscillations in a FAIMS cycle are proportionately smaller. This decreases resolution and raises the ion current ceiling (Figure 6), just as increasing the frequency or the gap width would.

This begs the question of whether one gas can be intrinsically superior to another. When g is reduced to 1.35 mm, I_{sat} in CO_2 decreases (at any DV) exactly to the level in N_2 (Figure 6a). The resolving power increases and now exceeds that in N_2 at equal ion current (Figure 6b). However, FWHM for g = 1.35 mm of CO_2 equals that for g = 2 mm of N_2, and the resolution improves only because CVs in CO_2 are higher as a consequence of *K*(*E*) for Cs^+ being steeper [7] in CO_2 than in N_2 (Table 1). For a hypothetical ion with identical CVs in N_2 and CO_2, the effect of exchanging the gas on FAIMS performance can always be cancelled by adjusting g and/or w_c. Hence the best intrinsic FAIMS separation of two ions will be provided by a gas in which the disparity between their CVs is greatest. Beyond that, the trade-off between resolution and sensitivity is fixed, whether

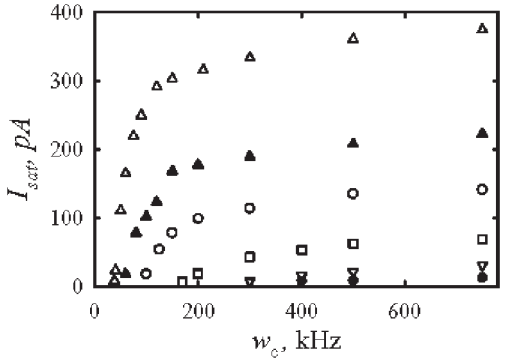

Figure 5. Same as Figure 3(**a**) at DV = −4.4 kV for $(H^+)_{12}$ bovine ubiquitin (empty symbols) and a hypothetical ion with mass and *K*(*E*) thereof, but q = 1 (filled symbols) at g = 2 mm (triangles), 1 mm (circles), 0.67 mm (squares), and 0.5 mm (inverted triangles).

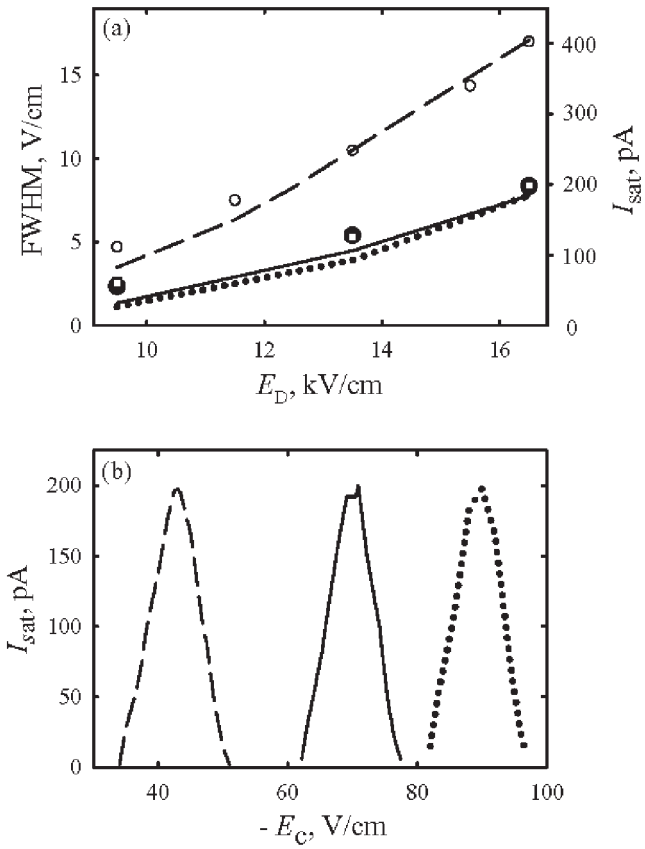

Figure 6. Simulated FAIMS response for Cs^+ in different buffer gases. In (**a**), lines are for transmitted current and circles are for peak width (FWHM): solid line/filled circles are in N_2 gas and dashed line/empty circles are in CO_2, both at g = 2 mm. The dotted line/empty squares are in CO_2 at g = 1.35 mm. In (**b**), CV peak profiles are simulated for three scenarios considered in (**a**) under the conditions yielding I_{sat} = 180 pA. Solid, dashed, and dotted lines correspond to same in (**a**).

managed via changing the gap width, the waveform frequency, or the buffer gas.

Analytical Gap Length and Gas Flow Velocity

The residence time of ions in the FAIMS gap, t_{res}, is proportional to its length (L) and inverse velocity of gas flow through it (v). Typical t_{res} in cylindrical FAIMS devices are 0.1–0.4 s. Most simulations in reference [37] and elsewhere in this paper assume t_{res} = 0.2 s. Thus, to utilize the separation peak capacity at R = 15–30, a CV scan with duty cycle of 90% would take a minute or more. Often this is too slow for online coupling with liquid-phase separations upfront.

We had already looked at the FAIMS response as a function of t_{res}, with the device geometry fixed and t_{res} controlled by gas flow velocity [37]. In that case, a longer t_{res} improves resolution while lowering sensitivity: ions are continually removed from the gap, with those located away from the median (that form the edges of peaks in CV spectra) depleted disproportionately [37]. Could other parameters be adjusted in concert with t_{res} such that the response is not affected? Since narrowing the gap increases resolution at the expense of sensitivity, reducing t_{res} and g (or w_c) simultaneously is an obvious direction. For (Leucine − H)$^-$ modeled here (Figure 7a), this solution works until t_{res} ≈30–40 ms, shorter times are not sufficient for proper separation and resolution is degraded. This could possibly be ameliorated by further narrowing the gap, but this step also decreases sensitivity. Regardless, the deterioration of performance cannot be compensated by varying g. This delineates an intrinsic limitation on FAIMS throughput due to minimum timescale of gas-phase separation. Still, Figure 6a suggests that analyses of midsize ions could be shortened about fivefold (without impairing quality) by proportional acceleration of gas flow. That would increase compatibility with online liquid-phase separations.

Another way to change t_{res} is by varying L at a fixed v. Again, the gap width could be adjusted simultaneously to keep sensitivity constant. In this case, resolution starts deteriorating already at t_{res} ~ 0.15 s (Figure 7b), and at any shorter t_{res} worsens significantly more than when equal t_{res} is achieved by increasing v at a

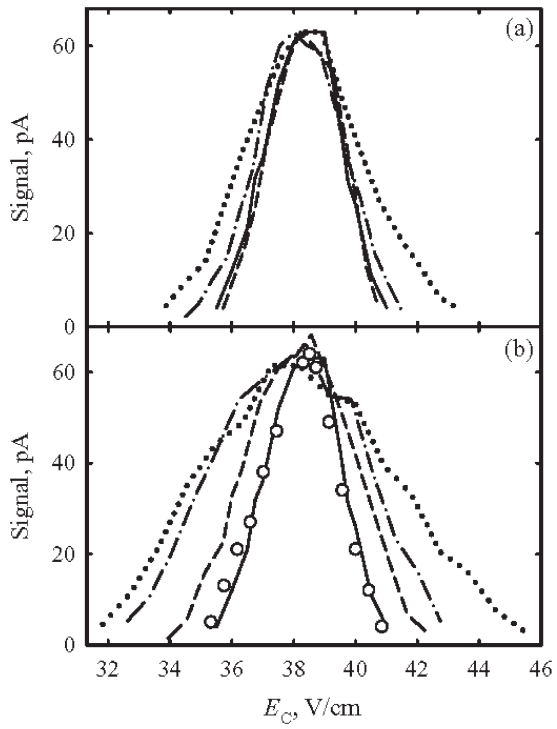

Figure 7. Simulated CV peak profile for (Leucine − H)$^-$ as a function of ion residence time: 1 s (circles), 0.2 s (solid line), 50 ms (dash), 20 ms (dash dot), and 10 ms (dotted). The value of t_{res} is controlled by the gas flow velocity in an analytical gap of fixed length (**a**) or by varying the length of a gap with constant gas flow (**b**). In (**a**), {t_{res}; g} sets are {0.2 s; 2.0 mm}, {50 ms; 1.31 mm}, {20 ms; 0.97 mm}, {10 ms; 0.79 mm}. The resolving power is ~13 at t_{res} ≥ 50 ms, ~11 at t_{res} = 20 ms, and ~8.5 at t_{res} = 10 ms. In (**b**), sets are {1.0 s; 2.35 mm}, {0.2 s; 2.0 mm}, {50 ms; 1.88 mm}, {20 ms; 1.38 mm}, {10 ms; 1.1 mm}. The resolving power is ~13 at t_{res} ≥ 0.2 s, ~9 at t_{res} = 50 ms, ~7 at t_{res} = 20 ms and ~5 at t_{res} = 10 ms. Values of g were chosen to ensure I_{sat} ~60 pA in all cases.

constant L. This non-equivalency would be expected: L is explicitly present (in addition to t_{res}) in the master equation governing ion dynamics in FAIMS [37]. Physically, larger v in a fixed geometry reduces charge density for a particular ion current, which increases I_{sat} and thus enhances sensitivity. That sensitivity gain allows a gap narrower than that for a fixed v (as is evident from the parameters quoted in caption of Figure 7), which improves resolution. The conclusion is that, for faster separations, accelerating the gas flow through FAIMS is preferable to shortening the device.

The initial distribution of ion coordinates is generally immaterial when modeling FAIMS separations for typical residence times because of randomization by ion focusing, diffusion, and Coulomb repulsion [37], but becomes important at shortest t_{res} that approach the timescales of those processes. Probing that issue is beyond the scope of this work, and the present findings regarding FAIMS performance for the shortest t_{res} should be deemed preliminary.

Optimization of Asymmetric Waveform Profile

Bisinusoidal Waveform

Most FAIMS work to date employed the waveform of eq 2 with high-to-low ratio f equal to 2. Some data were obtained [12, 13, 17, 19, 21, 24, 45] at $f = 3$ and 4, but no optimization of f has been pursued in either experiment or theory. Eq 2 reduces to a single sinusoidal and no separation occurs at either $f \rightarrow 0$ or $f \rightarrow \infty$, hence an optimum finite f must exist. Modeling for (Leucine − H)$^-$ shows that $f \sim 2$ provides the best transmission at both low and high ion currents (Figure 8a), though the maximum is not sharp. The resolution marginally improves as f increases (Figure 8b), likely because waveform changes (Figure 1a) augment the amplitude of oscillations in FAIMS cycle which effectively narrows the gap. For the same cost in sensitivity, this improvement is less than that produced by decreasing the gap or waveform frequency (Figure 3). For example, reducing w_c at $f = 2$ from 210 kHz to 125 kHz halves I_{sat} and increases R by ~30% (Figure 3b), while changing to $f = 4$ at $w_c = 210$ kHz also halves I_{sat} but increases $R < 10\%$ (Figure 8b). Then one should apply the waveform with $f \sim 2$ for best sensitivity, and, if desired, improve resolution as outlined in the preceding section.

Rectangular Waveform

It is believed that the ideal waveform for FAIMS analyses is not sinusoidal-based, but a rectangular one of eq 3, Figure 1b. The form of eq 2 (adopted as a practical compromise for simple implementation in RF circuitry) is less "asymmetric", which reduces the ion focusing force in cylindrical FAIMS. Other factors held constant, a stronger focusing by rectangular waveform would normally improve ion transmission. For example, at typical $g = 2$ mm and w_c of 210 or 750 kHz, sensitivity for (Leucine − H)$^-$ roughly doubles (Figure 9a). Under "highly constrained" conditions with a frequency near the cutoff for particular g, switching to a waveform of eq 3 decreases transmission because of a greater ion oscillation amplitude during FAIMS cycle. This raises the w_c cutoff, e.g., from ~80 kHz to ~110 kHz in Figure 9a.

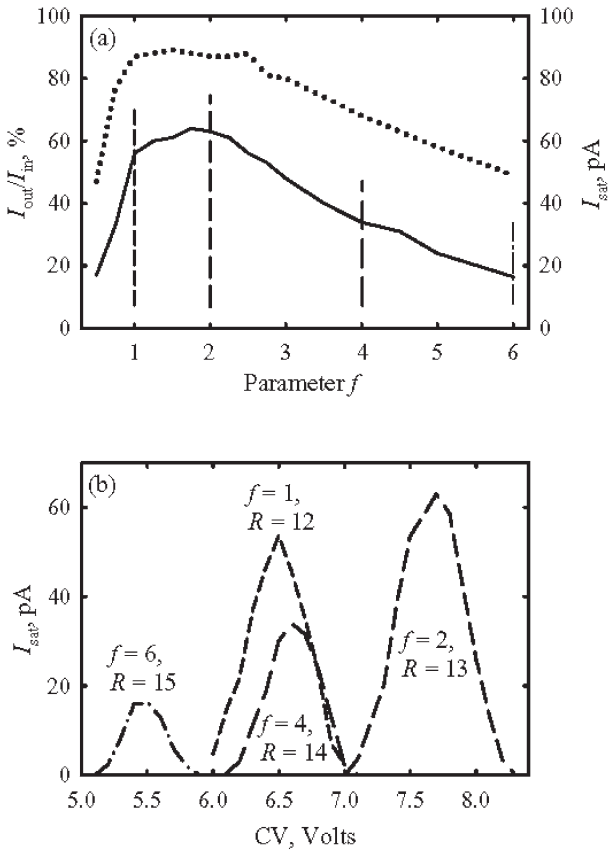

Figure 8. Sensitivity and resolution simulated for (Leucine − H)$^-$ as a function of f that defines bisinusoidal waveforms (Figure 1a). Panel (**a**) shows the transmission efficiency at $I_{in} \rightarrow 0$ (dotted line, left scale) and transmitted ion current (solid line, right scale), (**b**) presents CV spectral features at several f indicated by matching dashed bars in (**a**). Calculated resolving powers are indicated.

Rectangular waveforms also outperform bisinusoidal ones in separation efficiency. For the same (Leucine − H)$^-$ example, the resolving power (at $w_c = 210$ kHz) increases by ~25% (to $R = 16$) while I_{sat} doubles from ~60 pA to ~120 pA (Figure 9b). The benefit of changing to a rectangular waveform becomes clearer if other parameters are adjusted simultaneously such that only resolution or sensitivity is improved. Like with waveforms of eq 2, narrowing the gap raises R at the expense of sensitivity. For example, reducing g from 2 to 1.8 mm halves I_{sat} from ~120 pA back to ~60 pA, but increases R from 16 to 22 (Figure 9b). Alternatively, widening the gap to 2.2 mm decreases R from 16 back to 13, but increases I_{sat} to ~180 pA (Figure 9b). Either outcome may be achieved with a fixed $g = 2$ mm by changing the frequency. Hence a transition from a bisinusoidal to a

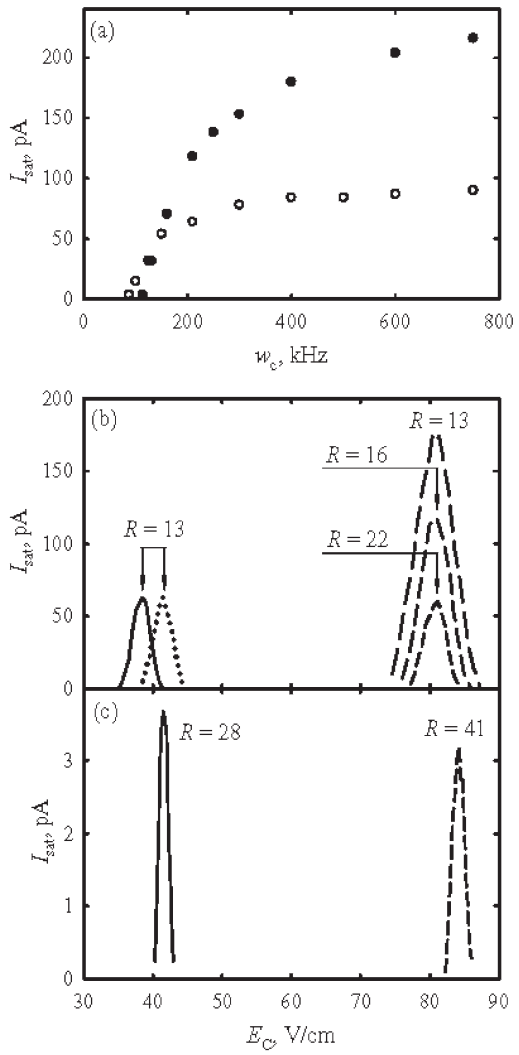

Figure 9. Sensitivity and resolution for (Leucine − H)$^-$ simulated for rectangular waveform (filled circles, dashed lines) versus bisinusoidal waveform (empty circles, solid line), both with $f = 2$. Panel (**a**) shows saturated current at $g = 2$ mm, $w_c = 210$ kHz. In (**b**), CV spectra are plotted at $w_c = 210$ kHz and $g = 2$ mm (solid and medium dash lines) and, for rectangular waveform, $g = 1.8$ mm (long dash) and 2.2 mm (short dash). Features in solid and short-dash lines have equal heights, those in solid and long dash lines have equal R. Dotted line is for the clipped-sinusoidal waveform at $w_c = 137$ kHz and $g = 2.05$ mm chosen to yield the same peak intensity. In (**c**), high-resolution CV spectra are shown at $g = 2$ mm, $w_c = 86$ kHz (solid line) and $w_c = 113.5$ kHz (dashed line). The two features have similar intensities. Calculated resolving powers are indicated.

rectangular waveform could improve resolution by 70% without loss of sensitivity, or triple sensitivity without affecting resolution. The maximum achievable resolving power also increases, e.g., for (Leucine − H)$^-$ from ~30 to ~40 at same $I_{sat} \sim 3.5$ pA (Figure 9c). These are significant gains that justify engineering a waveform close to the ideal, despite a greater complexity or cost.

What is the optimum ratio f for a rectangular waveform? Simulations suggest that transmitted (Leucine − H)$^-$ ion current maximizes at $f \sim 3.5$ (Figure 10a), rather than $f \sim 2$ for waveforms of eq 2. This arises because an equal increase of f diminishes the oscillation amplitude during a cycle of rectangular waveform (Figure 1b) more than for a bisinusoidal one (Figure 1a). In effect, the gap widens at higher f, which should improve sensitivity but degrade resolution. Indeed, the value of R drops from 16 at $f = 2$ to $R = 12$ at $f = 3.5$ (Figure 10b). As found above, one could achieve both higher I_{sat} (~180 pA versus ~165 pa) and better R (13 versus 12) using $f = 2$ and $g = 2.2$ mm. Hence the operation at $f = 3.5$ is intrinsically inferior to that at $f = 2$. At $f > 3.5$, both resolution and sensitivity worsen. For the same reason, reducing f below 2 improves resolution but decreases sensitivity (Figure 10a, b). Again, a better trade-off between resolution and sensitivity could be obtained by narrowing the gap at $f = 2$ instead. Thus the optimum f is still two, same as for bisinusoidal waveforms.

Clipped sinusoidal waveform

Recently Buryakov et al. [39–42] have introduced a new FAIMS waveform of eq. (4), generated by clipping a single sinusoidal offset by a fixed DC voltage. Present modeling for (Leucine − H)$^-$ shows this and bisinusoidal waveforms to produce a near-identical performance (Figure 9b). The resolution obtained in reference [39] was relatively high, from $R \sim 18$ for trinitrotoluene anion to $R \sim 34$ for iodide. Present model reproduces those values virtually exactly: the example of I^- is presented in Figure 11 (assuming $t_s = 2.7$ ms and $t_c = 7.3$ ms—the midpoint of $t_c = 6.8$–7.8 ms range used in

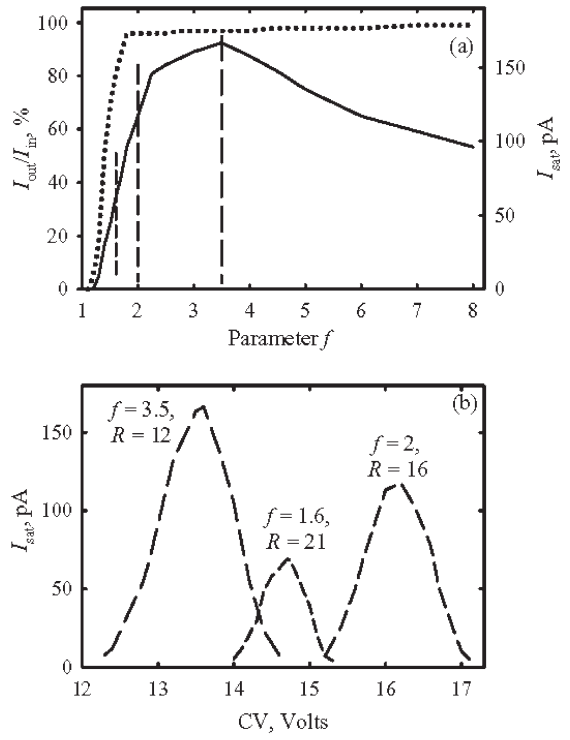

Figure 10. Same as Figure 8 for rectangular waveforms (Figure 1b).

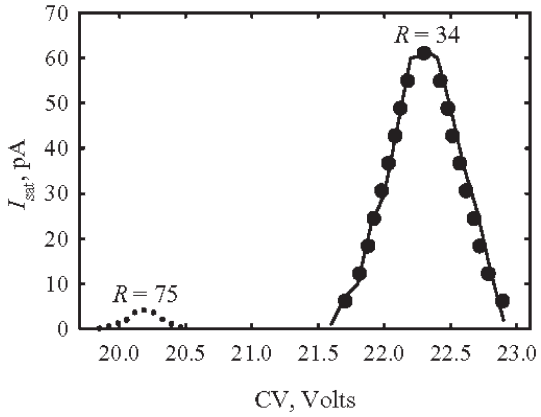

Figure 11. Simulated (lines) and measured (circles, reference [39]) peak profiles for I^-. Solid line is for clipped-sinusoidal waveform with w_c = 137 kHz used in reference [39], dotted line is for bisinusoidal waveform with w_c = 117 kHz and same g = 2 mm. Calculated resolving powers are indicated.

[39]). Hence a high resolution in reference [39] is achieved not by a novel waveform, but by a low frequency (w_c = 137 kHz) via the mechanism described earlier. As expected, sensitivity under these conditions is modest [39]. Calculations predict that a still lower frequency would improve the resolution further, e.g., up to $R \sim 75$ at w_c = 117 kHz (Figure 11). Yet higher R would be attainable with a rectangular waveform. An excellent agreement between present simulations and measurements supports the notion of balancing FAIMS resolution and sensitivity performance by adjusting the waveform frequency.

Conclusions

Recently we described [37] a numerical simulation of FAIMS analyzers (in essence a SIMION-type approach for FAIMS) that involves propagating an ensemble of ion trajectories through those devices under realistic conditions, accounting for the ion diffusion (including high-field and anisotropic components) and Coulomb repulsion. Here, this model was further validated and employed to optimize the resolution, sensitivity, and throughput of cylindrical FAIMS as a function of instrumental parameters.

As is common in mass spectrometry, and especially quadrupole MS to which FAIMS is often compared, one can trade off resolution and sensitivity. This trade-off may be adjusted widely by varying the analytical gap width or (equivalently) the waveform frequency. Another option involves changing the buffer gas, though this is equivalent to first two modes only for ions that have equal nonlinear mobility coefficients in two gases (while absolute mobilities differ). In particular, calculations have identified parameter settings that should double or triple the resolution at practical ion currents, which would improve FAIMS utility in many applications significantly. For example, resolving powers could be raised from the current 10–15 to ~25–30 for mid-size species such as Leucine and from ~25–35 to ~75 for smallest ions like Iodide. Separations for typical analytes are predicted to be accelerated at least several times with minimal effect on performance by speeding the gas flow through analytical gap. This would reduce the timescale of FAIMS analyses, thus improving the coupling to LC and other liquid-phase separations. Shortening the analytical gap also reduces that timescale, but at a higher price in terms of quality. Optimization of the asymmetric waveform has shown an essentially equal merit of bisinusoidal and clipped sinusoidal waveforms used in existing devices, but a substantial advantage of a rectangular profile over both, in terms of resolution and/or sensitivity. In particular, maximum FAIMS resolution could be improved by over a third. With both sinusoidal-based and rectangular waveforms, the device performance maximizes when the voltage during "high" part of the cycle is about twice that during the "low" part.

FAIMS separations are governed by a fine interplay of multiple mechanical and operational parameters. We make no claim of achieving a "global optimization" for FAIMS analyzers, especially since the desired optimum depends on specific priorities. Optimal parameters will also depend on the analyte, and may differ substantially for species with properties far from those of ions considered in this work. Rather, we expect the present mapping of major trends as a function of key experimental variables to steer further development and application of FAIMS technology. Finally, several important factors were omitted from our analysis, e.g., the cylindrical curvature radius that controls the strength of ion focusing and thus greatly affects both resolution and sensitivity. We also did not study the effects of altering the cylindrical geometry, for example, by an added hemispherical element found in some commercial FAIMS devices. Those potential avenues to continued improvement of FAIMS capabilities will be explored in future work.

Acknowledgments

The authors thank Dr. R. Guevremont and Dr. R. Purves (Ionalytics Corporation), and Professor J. de la Mora (Yale University), for sharing their unpublished results and for extensive discussions of FAIMS design and operation. They also thank the U.S. Department of Energy (PNNL Laboratory Directed Research and Development Program) and the NIH National Center for Research Resources (RR18522) for supporting portions of this research. Pacific Northwest National Laboratory is operated by the Battelle Memorial Institute for the U.S. Department of Energy through contract DE-ACO6-76RLO1830.

References

1. Buryakov, I. A.; Krylov, E. V.; Soldatov, V. P. U.S.S.R. Inventor's Certificate no. 1485808; 1989.
2. Buryakov, I. A.; Krylov, E. V.; Nazarov, E. G.; Rasulev U. K. *Int. J. Mass Spectrom. Ion Processes* **1993,** *128*, 143.
3. Carnahan, B. L.; Tarassov, A. S. U.S. Patent no. 5420424; 1995.

4. Purves, R. ; Guevremont, R.; Day, S.; Pipich, C. W.; Matyjaszczyk, M. S. *Rev. Sci. Instrum.* **1998,** *69*, 4094.
5. Guevremont, R.; Purves, R. W. *Rev. Sci. Instrum.* **1999,** *70*, 1370.
6. Handy, R.; Barnett, D. A.; Purves, R. W.; Horlick, G.; Guevremont, R. *J. Anal. At. Spectrom.* **2000,** *15*, 907.
7. Barnett, D. A.; Ells, B.; Guevremont, R.; Purves, R. W.; Viehland, L. A. *J. Am. Soc. Mass Spectrom.* **2000,** *11*, 1125.
8. Guevremont, R.; Barnett, D. A.; Purves, R. W.; Viehland, L. A. *J. Chem. Phys.* **2001,** *114*, 10270.
9. Ells, B.; Barnett, D. A.; Purves, R. W.; Guevremont, R. *J. Environ. Monit.* **2000,** *2*, 393.
10. Ells, B.; Barnett, D. A.; Froese, K.; Purves, R. W.; Hrudey, S.; Guevremont, R. *Anal. Chem.* **1999,** *71*, 4747.
11. Barnett, D. A.; Guevremont, R.; Purves, R. W. *Appl. Spectrosc.* **1999,** *53*, 1367.
12. Ells, B.; Barnett, D. A.; Purves, R. W.; Guevremont, R. *Anal. Chem.* **2000,** *72*, 4555.
13. Ells, B.; Froese, K.; Hrudey, S. E.; Purves, R. W.; Guevremont, R.; Barnett, D. A. *Rapid Commun. Mass Spectrom.* **2000,** *14*, 1538.
14. Eiceman, G. A.; Tarassov, A.; Funk, P. A., Hughs, S. E.; Nazarov, E. G.; Miller, R. A. *J. Sep. Sci.* **2003,** *26*, 585.
15. McCooeye, M. A.; Ells, B.; Barnett, D. A.; Purves, R. W.; Guevremont, R. *J. Anal. Toxicol.* **2001,** *25*, 81.
16. McCooeye, M. A.; Mester, Z.; Ells, B.; Barnett, D. A.; Purves, R. W.; Guevremont, R. *Anal. Chem.* **2003,** *74*, 3071.
17. Gabryelski, W.; Wu, F.; Froese, K. L. *Anal. Chem.* **2003,** *75*, 2478.
18. McCooeye, M.; Ding, L.; Gardner, G. J.; Fraser, C. A.; Lam, J.; Sturgeon, R. E; Mester, Z. *Anal. Chem.* **2003,** *75*, 2538.
19. Gabryelski, W.; Froese, K. L. *Anal. Chem.* **2003,** *75*, 4612.
20. Cui, M.; Ding, L.; Mester, Z. *Anal. Chem.* **2003,** *75*, 5847.
21. Guevremont, R.; Barnett, D. A.; Purves, R. W.; Vandermey, J. *Anal. Chem.* **2000,** *72*, 4577.
22. Barnett, D. A.; Purves, R. W.; Ells, B.; Guevremont, R. *J. Mass Spectrom.* **2000,** *35*, 976.
23. Guevremont, R.; Purves, R. W.; Barnett, D. A.; Ding, L. *Int. J. Mass Spectrom.* **1999,** *193*, 45.
24. Guevremont, R.; Ding, L.; Ells, B.; Barnett, D. A.; Purves, R. W. *J. Am. Soc. Mass Spectrom.* **2001,** *12*, 1320.
25. Barnett, D. A.; Ells, B.; Guevremont, R.; Purves, R. W. *J. Am. Soc. Mass Spectrom.* **1999,** *10*, 1279.
26. Purves, R. W.; Barnett, D. A.; Ells, B.; Guevremont, R. *Rapid Commun. Mass Spectrom.* **2001,** *15*, 1453.
27. Purves, R. W.; Guevremont, R. *Anal. Chem.* **1999,** *71*, 2346.
28. Purves, R. W.; Barnett, D. A.; Ells, B.; Guevremont, R. *J. Am. Soc. Mass Spectrom.* **2000,** *11*, 738.
29. Purves, R. W.; Barnett, D. A.; Ells, B.; Guevremont, R. *J. Am. Soc. Mass Spectrom.* **2001,** *12*, 894.
30. von Helden, G; Wyttenbach, T.; Bowers, M. T. *Science* **1995**, *267*, 1483.
31. Shvartsburg, A. A.; Hudgins, R. R.; Dugourd, P.; Jarrold, M. F. *Chem. Soc. Rev.* **2001,** *30*, 26.
32. Srebalus Barnes, C. A.; Hilderbrand, A. E.; Valentine, S. J.; Clemmer, D. E. *Anal. Chem.* **2002**, *74*, 26.
33. Asbury, G. R.; Hill, H. H. *J. Micro. Sep.* **2000,** *12*, 172.
34. Shen, Y. F; Zhao, R.; Berger, S. J.; Anderson, G. A.; Rodriguez, N.; Smith, R. D. *Anal. Chem.* **2002,** *74*, 4235.
35. Issaeva, T.; Kourganov, A.; Unger, K. *J. Chromatogr. A* **1999,** *846*, 13.
36. Dahl, D. A. *Int. J. Mass Spectrom.* **2000,** *200*, 3.
37. Shvartsburg, A. A.; Tang, K.; Smith, R. D. *J. Am. Soc. Mass Spectrom.* **2004,** *15*, 1487.
38. Shvartsburg, A. A.; Tang, K.; Smith, R. D. *Anal. Chem.*, in press.
39. Buryakov, I. A. *Talanta* **2003,** *61*, 369.
40. Buryakov, I. A. *J. Chromatogr. B* **2004,** *800*, 75.
41. Buryakov, I. A.; Kolomiets, Y. N.; Luppu, V. B. *J. Anal. Chem.* **2001,** *56*, 336.
42. Buryakov, I. A. *Tech. Phys.* **2002,** *47*, 1453.
43. Tang, K.; Page, J. S.; Smith, R. D. *J. Am. Soc. Mass Spectrom.* **2004,** *15*, 1416.
44. Tolmachev, A. V.; Udseth, H. R.; Smith, R. D. *Anal. Chem.* **2000,** *72*, 970.
45. Gabryelski, W.; Froese, K. L. *J. Am. Soc. Mass Spectrom.* **2003,** *14*, 265.
46. Eisele, F. L.; Perkins, M. D.; McDaniel, E. W. *J. Chem. Phys.* **1981,** *75*, 2473.
47. Perkins, M. D.; Eisele, F. L.; McDaniel, E. W. *J. Chem. Phys.* **1981,** *74*, 4206.
48. Eiceman, G. A.; Nazarov, E. G.; Stone, J. A. *Anal. Chim. Acta* **2003**, *493*, 185.
49. Li, J. W.; Taraszka, J. A.; Counterman, A. E.; Clemmer D. E. *Int. J. Mass Spectrom.* **1999,** *187*, 37.
50. Thackston, M. G.; Eisele, F. L.; Ellis, H. W.; McDaniel, E. W. *J. Chem. Phys.* **1977,** *67*, 1276.
51. Rokushika, S.; Hatano, H.; Hill, H. H. *Anal. Chem.* **1986,** *58*, 361.
52. Byers, M. S.; Thackston, M. G.; Chelf, R. D.; Holleman, F. B.; Twist, J. R.; Neeley, G. W.; McDaniel, E. W. *J. Chem. Phys.* **1983,** *78*, 2796.
53. Perkins, M. D.; Chelf, R. D.; Eisele, F. L.; McDaniel, E. W. *J. Chem. Phys.* **1983,** *79*, 5207.